X-625-76-24
PREPRINT

VARIATIONAL ELECTRIC FIELDS AT LOW LATITUDES AND THEIR RELATION TO SPREAD F AND PLASMA IRREGULARITIES

J. A. HOLTET
N. C. MAYNARD
J. P. HEPPNER

JANUARY 1976

GSFC — GODDARD SPACE FLIGHT CENTER —
GREENBELT, MARYLAND

VARIATIONAL ELECTRIC FIELDS AT LOW LATITUDES AND THEIR RELATION TO SPREAD F AND PLASMA IRREGULARITIES

J. A. Holtet*, N. C. Maynard and J. P. Heppner
Laboratory for Planetary Atmospheres
Goddard Space Flight Center
Greenbelt, Maryland 20771, U.S.A.

January 1976

*NAS-NRC Research Associate. Present Address: The Norwegian Institute of Cosmic Physics, Blindern, Oslo 3, Norway

ABSTRACT

Recordings from OGO 6 show that electric field irregularities are frequently present between ± 35° geomagnetic latitude in the 2000 - 0600 local time sector. The signatures are very clear, and are easily distinguished from the normal AC background noise, and whistler and emission activity. The spectral appearance of the fields makes it meaningful to distinguish between 3 different types of irregularities. Type A: Strong irregularities, typically 5-10 $\mu Vm^{-1}Hz^{-\frac{1}{2}}$ at 10 Hz, where the spectrum follows a power law $A \propto f^{-n}$, $n = 1.2 \pm 0.2$. Small DC electric field fluctuations are often observed at the same time. Type B: Weak irregularities, 0.5-1 $\mu Vm^{-1}Hz^{-\frac{1}{2}}$ at 10 Hz, with a more flat spectrum, $A \propto f^{-n}$, $0 < n < 0.5$. Type C: Weak irregularities with a rising spectrum, $A \propto f^{+n}$, $n > 0$, typical amplitudes 0.5-1 $\mu Vm^{-1}Hz^{-\frac{1}{2}}$ at 500 Hz. Type A irregularities seem most likely to occur in regions where gradients in ionization are present. Changes in plasma composition, resulting in an increase in the mean ion mass, are also often observed in the irregularity regions. Comparison with ground based ionosondes indicates a connection between Type A irregularities and low latitude spread F. A good correlation is also present between Type A fields and small scale fluctuations in ionization, $\Delta N/\overline{N} > 1\%$. From the data it appears as if a gradient driven instability is the most likely source of the Type A irregularities. Type B and C irregularities are more difficult to relate to other measured variations in the surrounding plasma. However, there seems to be some connection between Type C fields and local depletions in ionization.

INTRODUCTION

The general irregular nature of the equatorial and low latitude F regions has been established by numerous observations since Booker and Wells (1938) first attributed diffuse echoes, observed by the Huancayo ionosonde, to scattering of the radio waves from irregular structures in the ionization. The major part of these data have been derived from various kinds of radio experiments, such as bottomside and topside sounding, VHF forward scatter and backscatter, and scintillations in signals from radio stars and orbiting satellites. During the last few years, in situ measurements of electric fields and thermal and suprathermal electron and ion densities, made from rockets and satellites, have also greatly contributed to the experimental understanding of these phenomena..

However, when it comes to direct comparison between measurements of various kinds, little has been done which goes beyond statistical studies. Thus, it is not quite clear whether the irregularities seen by different experimental methods all have their background in the same geophysical phenomenon, or which kinds of irregularities will be meaningful to relate to the same source.

The present work is based on in situ measurements of variational electric fields at low latitudes, made by the OGO 6 satellite. These observations will be compared with other data on F region structures, to see how the electric field fluctuations fit into the general picture of low latitude irregularities, both from the experimental side, and possible processes for generation of the irregularities.

THE OGO 6 ELECTRIC FIELD EXPERIMENT

The OGO 6 satellite, with its slightly elliptical polar orbit (400 to 1100 km, inclination $\sim 82^{\circ}$), was particularly well fitted for studies of upper F region phenomena. The electric field measurements were based on the double probe technique using long cylindrical antennas (Aggson, 1969). Electric fields from DC to approximately 500 kHz could be monitored by two experiments sharing the probes. The data which will be discussed are all from the low frequency, DC/ELF-experiment (for results from the VLF/LF experiment cf. works by Laaspere et al., e.g. 1971; 1973). This instrumentation was designed to record field amplitudes from DC to 4 kHz. The measurements were made within 7 different bands: a DC channel, an AC coupled "Quasi-DC" channel (time constant 60s) for observing small scale variations in the DC field, and 5 filter channels which measured variational fields at higher frequencies. The 10 dB points, where neighboring filters overlapped, were at 4-16-64-256-1024-4096 Hz. The sensitivities of the four lowest AC channels were all better than 1 μVm^{-1} integrated amplitude over the bandwidth, with baseline noise levels of 0.18 $\mu Vm^{-1}Hz^{-\frac{1}{2}}$ in channel #1 (4-16 Hz) decreasing to 0.027 $\mu Vm^{-1}Hz^{-\frac{1}{2}}$ in channel #4 (256-1024 Hz). The sensitivity of channel #5 was somewhat reduced due to spacecraft interference. The output amplifiers had a logarithmic response with ~ 60 dB dynamic range. Each channel was sampled at a rate of approximately 1 Hz. Internal time constants were chosen so that the response was always faster than the data rate. (For more details about the DC part of the experiment cf. Heppner, 1972; Maynard, 1974).

After the first period of operation (June 9-22, 1969), when the orbit was in the dawn-dusk sectors, a fault in the solar power system shifted the spacecraft potential and caused saturation of the instrument whenever the satellite was in sunlight. Thus, for the major part of its lifetime, data could only be obtained when the spacecraft was eclipsed from the sun by the earth. Except for this limitation in covering local times, and the sensitivity limitation above 1 kHz mentioned previously, the experiment worked satisfactorily.

OBSERVATIONS - GENERAL INTRODUCTION

As an introduction to the data a full polar pass from the equator on the dusk-side, over the polar cap and down through the dawn-side equatorial region is shown in Figures 1A and B. This will place the equatorial data in a context where they can be viewed together with observations made at other latitudes.

In analyzing these data, one should consider the two highest filter channels separately from the two low ones. The amplitude variations in the two high channels result from well known electromagnetic wave phenomena such as whistlers or ELF chorus and hiss (cf. e.g. Taylor and Gurnett, 1968; Muzzio and Angerami, 1972). In the two low filter channels the field amplitude stays at a very low level throughout the dusk-side equatorial and low latitude region until it rather suddenly rises above the detection level at 0833:30 UT ($L \approx 2.7$). From here on the noise fields, as seen by the two detectors below 64 Hz, go through the following pattern, which is very typical for a polar pass. First the field fluctuations stay at medium intensity ($\sim 10\ \mu Vm^{-1}$ integrated

amplitude) in the sub-auroral region until the field strength increases as the satellite passes through the auroral oval. Inside the polar cap the field amplitudes are again at a moderate level. After an enhanced field appears in the dawn auroral oval crossing, the field then decays to a medium intensity in the sub-auroral region with a rather sudden low latitude cut-off, seen at approximately 0853:40 UT ($L \approx 2.8$). Thus, a low frequency electric field is present more or less continuously poleward from its first appearance in the sub-suroral region. Similar auroral zone enhancements seen by the less sensitive OV1-10 satellite instrument were used by Heppner (1969) and Maynard and Heppner (1970) to define average auroral zone boundaries.

Thus three high latitude regions are evident. A sub-auroral belt exists with moderate intensity fields, often with a very sharp low latitude boundary. In the auroral oval the fields reach their peak amplitudes; field strengths as high as 300 $\mu Vm^{-1}Hz^{-\frac{1}{2}}$ at 10 Hz are not uncommon. The sub-auroral belt may sometimes be separated from the auroral oval by a region with reduced field amplitudes. Inside the polar cap the field amplitude is usually much lower than in the auroral oval. In all three regions the amplitude fluctuations in time and/or space may be very large.

The amplitude vs. frequency spectra of the noise fields are different in each of the regions. Figure 2 shows spectra from a typical pass. In the auroral oval the amplitude variation follows approximately a $f^{-1.4}$ curve, or roughly a 1/f variation. Inside the polar cap the spectrum is more flat, more like $f^{-\frac{1}{2}}$, while the sub-auroral belt has a flat spectrum

in the low frequency part and then a more rapid fall off in the high frequency tail (it should, however, be pointed out that the determination of the high frequency points in the sub-auroral belt is often uncertain, since these noise fields usually are riding on a background of ELF hiss). Comparison with data from the OGO 6 search coil experiment (E. Smith, personal communication, 1975 shows that, with the exception of some noise peaks which occur in the auroral oval, all these fields are primarily electrostatic in nature.

Returning to Figure 1B again, it can be seen that after leaving the sub-auroral belt, the amplitude stays at the background noise level until, when at very low latitudes, the satellite passes through several belts with enhanced low frequency fields. Figure 3 shows another example where the same type of low latitude fields are present. Typical amplitude spectra of such irregularities (shown in Figure 4) fall off with frequency as $f^{-1.2 \pm 0.2}$, similar to spectra in the auroral zone. We will in the following refer to these noise fields as Type A irregularities, (strong irregularities with roughly a 1/f spectrum). This type of AC field variations has also been seen by the OV1-17 satellite (Kelley and Mozer, 1972).

If we consider the last structured region in Figure 1B located approximately at the dip equator, we notice that this also includes some amplitude fluctuations at higher frequencies which do not correspond to the variations seen in the Type A fields. Figure 5 shows a cleaner case of this noise, which here is seen undisturbed by, and unrelated to, a Type A event. The amplitude is much lower than in Type A, and in our

representation, with amplitude detection over two-octave bands, the field appears with approximately the same value in all channels. The amplitude spectrum, however, has a slope, $A \tilde{\propto} f^{-\frac{1}{2}}$ (see example in Figure 6). We will designate irregularities with such spectra Type B irregularities. Note that while Type B irregularities have a similar frequency spectrum to signals seen in the polar cap, they are more regular, exhibiting much less structure.

A third group of AC fields found near the equator is shown in Figure 7. These fields, which we will term Type C, differ from the two other groups mainly by having an amplitude spectrum where $|\underline{E}(1000 \text{ Hz})| > |\underline{E}(100 \text{ Hz})|$, or in other words, in the region 100-1000 Hz the amplitude spectrum will have a slope $\propto f^{+n}$, where n is a small number > 0.

A comparison with AC magnetic field data (E. Smith, personal communication, 1975) shows no corresponding counterpart to any of these three types of low latitude AC electric fields so that one can conclude that all are electrostatic.

One implication of the electrostatic nature of the signals is that the frequencies measured are Doppler-shifted up to where they are observed, since v (satellite) $\gg v_{ph}$ for the electrostatic wave, and it would therefore perhaps be more meaningful to talk about dimensions and k-spectra instead of frequency spectra. However, since the measurements are made in the frequency domain, that is what we will use in this paper, realizing that a 10 Hz frequency seen by the satellite corresponds to 800 m structures, and a 1 kHz signal to 8 m structures. A second implication is that the antenna length will be longer than the dimensions of the fields at the

highest frequencies. This will reduce the sensitivities and make the conversions from potential differences to field strengths somewhat incorrect. Thus, a correction factor technically should be applied to field amplitudes above approximately 450 Hz. Since this correction has not been applied, it should be kept in mind that the amplitudes stated for the two upper channels will be somewhat underestimated. However, this is not of consequence in the conclusions.

In summary, the data reveal that the electrostatic wave fields which are observed in the low latitude F-region can be grouped in three different classes, based on spectral characteristics: Type A - strong 1/f irregularities, Type B - weak irregularities with a "flat spectrum", and Type C - equatorial hiss or weak irregularities with a rising spectrum. Types A and B are similar in spectral character to irregularities seen in the auroral region and polar cap region respectively.

THE STRONG 1/f IRREGULARITIES - TYPE A

When the strong Type A irregularities are present they are usually found between $\pm$ 35° magnetic latitude. In one pass the satellite may cut through several highly structured irregularity regions (Figure 1B), or it may stay inside one continuous region which extends over tens of degrees in latitude. In a pass from one hemisphere to another there is usually no evidence of conjugacy in the structures; however, the spacecraft in general does not stay on the same magnetic longitude throughout the low latitude region. A transition into a strong irregularity field may be very sudden, over a distance of $\sim$ 10 km, or it can be more gradual. Both types of amplitude variations may be seen within a region of irregularities.

The Type A irregularities have been observed in the nightside and in the early morning sector, but not in the dusk sector. Although there are limitations in local time coverage of the data, it appears that Type A fields are nighttime phenomena which extend into the sunlit morning sector.

The irregularities are observed within the entire altitude range spanned by the spacecraft, but are more frequently present below 700 km than above. This is illustrated in Figure 8. Here the heavy lines represent regions with Type A fields. Lightly drawn lines or no lines, in the case of the continuation of an orbit to higher L values, represent regions without Type A fields. A short light curve indicates a pass with no activity. The data used in this figure are from the period October - November 1969. All equatorial passes are from the African-American longitudinal sector, and all are from periods with low geomagnetic activity. The concentration of Type A passes on the left hand side of the plot indicates that the occurrence of the irregularities is altitude controlled, rather than being localized to particular magnetic L-shells. Or, in other words, a position at low altitude and "high" L, e.g. 400 km and L = 1.2, is more favorable for observation of irregularities than at high altitude (e.g. 1000 km) with the same L value. Thus, the irregularities are not necessarily propagated up magnetic lines of force. There is, however, one reservation. Since the data used for this figure also scans local times from $\sim$ 2200 at the lowest altitudes to $\sim$ 0300 at the highest altitudes, a local time dependence may also be present. It has not been possible to completely exclude this possibility, but the data appear to support the conclusion

that this is an altitude rather than L dependence in occurrence. No clear relation, neither correlation nor anticorrelation, between the Type A fields and magnetic activity has been found.

An attempt has been made to correlate the AC electric field structures with low latitude spread F, as observed by ground based ionosondes. Ionosonde data from an extensive network of stations were obtained from the World Data Center A, in the form of hourly values of the FOF2 (observed ordinary-wave penetration frequency of the F2 layer). Presence of spread echoes in the data is here noted with the descriptive letter F (Piggott and Rawer, 1972). These data only give information about spread F on an hour to hour basis. Generally, spread F will exist more frequently than indicated by the hourly values. Furthermore, no details as to the type of echoes and in which height interval the spreading appeared are given. This, together with the displacement in time and space usually present between satellite and ground based observations, makes the comparison more of a statistical nature than a series of event studies.

Figures 9 and 10 show two examples of the types of plots produced to examine spread F correlation. In a geographical coordinate grid the satellite trajectory is drawn together with the envelope of the amplitude variations in channel #1 on the right hand side of the trajectory, and one of the high frequency channels (3 or 4) on the left hand side. The UT at the start of the pass is given at the beginning of the curve. Dashed orbit lines indicate data gaps. The magnetic dip equator is drawn as a heavy line. The coding of the spread F data is the following: a triangle represents a station which had the descriptive letter F in the hour interval where

the satellite pass occurred and a circle is a station without spread F. Figure 9 represents data from the northern hemisphere summer with local times ~ 0600. Figure 10 is from the northern winter, with local times ~ 2200. Both data sets are from low altitudes. In Figure 9 there is very little spread F observed by the ground network, and there is also very little Type A activity in the longitudinal sector ± 120°. In the West-Pacific sector, where Type A activity is present, we do not have sufficient ground stations to cover the satellite adequately. In the data sets in Figure 10 all the African ionosondes near the equator showed spread F, a feature which was present during most of the night, and the satellite data also show Type A electric fields in all passes in the African-Atlantic sector. In the Indian-Pacific sector spread F is scarcely observed and the E-field data do not show Type A events.

The conclusion from these and other correlations with spread F is that the occurrence of Type A electric fields and spread F seems to be related. Even though cases are found which seem to be in disagreement with this conclusion, they could easily be a result of the displacement in time and space between the satellite and ionosonde measurements. Another feature which is illustrated by Figures 9 and 10 is that in going from northern hemisphere summer (Figure 9) to northern winter (Figure 10) there is a longitudinal shift of the region where Type A events most frequently occur. In northern summer these fields are most frequently observed in the Pacific-Indian longitudinal sector. In northern winter the region of maximum occurrence is shifted over to the African-American Sector.

Looking at other parameters observed from the same spacecraft, we first of all notice that Type A AC irregularities very often are accompanied by a low amplitude DC field (cf. Figures 1B and 3). Comparisons between field irregularities and measurements of plasma density and composition seem to establish that the Type A fields tend to occur in regions where gradients in ionization density are observed (W. B. Hanson, and J. P. McClure, personal communication, 1975, H. A. Taylor, personal communication, 1975). Furthermore, a change in the plasma composition which results in an increase in the mean ion mass often appears in the irregularity regions, so that this seems to increase the probability for the production of electric field irregularities (Figure 11).

On a smaller scale the Type A events appear to be well correlated with ionization irregularities observed by the OGO 6 retarding potential analyzer (Hanson et al., 1970, Dyson et al., 1974). The AC irregularity regions correspond to a very high degree to regions where the fluctuations in ionization density $\Delta N/\overline{N}$, reach a rms value > 1%. Even though the time resolution in the two data sets is different, so that comparisons of fine structure are not possible, the overall regions (including the larger scale variations) correspond very well (cf. Figures 11 and 12). Hence, it can be concluded that there is a relation between the Type A electric fields and small scale ionization irregularities. This statement has to be weakened somewhat for the dawn sector. Near the terminator, other types of ionization irregularities also seem to be present, and cases exist, as the one shown in Figure 13, where a $\Delta N/\overline{N}$ irregularity can be seen without a corresponding variation in the AC electric field.

In summary, Type A AC electric fields (strong irregular signals with approximately a 1/f amplitude spectrum) seem to be correlated with equatorial spread F. The AC fields are often observed in connection with weak DC fields, and they appear to be generated in regions where gradients in ionization density are present, and/or where the ion composition is changed in such a way that the mean ion mass is increased. A good correlation between the field irregularities and small scale ionization irregularities exists on the nightside.

TYPE B IRREGULARITIES - WEAK IRREGULARITIES WITH A "FLAT" AMPLITUDE SPECTRUM

The Type B equatorial AC field was defined, and distinguished from the Type A, by its spectral appearance: a rather flat amplitude spectrum, $A \tilde{\propto} f^{-\frac{1}{2}}$, The Type B fields are much weaker (order of magnitude) than the Type A in the low frequency components, but because of the different slopes of the spectra Type B will have stronger high frequency components. Typical amplitudes are 0.5 - 1 $\mu Vm^{-1}Hz^{-\frac{1}{2}}$ at 10 Hz.

The Type B events seem to occur more frequently in the early morning sector than in the night. They are more closely tied to the equatorial region ($\pm$ 15°) than the Type A fields, and are also seen to be less structured in time or space. Typical Type B passes can be seen in Figures 5 and 13. Going from a latitude of approximately + or - 15° toward the equator the amplitude slowly builds up and then changes to more fluctuating structures in the equatorial region, resembling two waves which appear on either side of the equator and break into an irregular ripple in the region where the two merge.

From the correlation studies with spread F it can be concluded that there is no connection between the Type B events and spread F echoes observed by ground based HF ionosondes. Also it has not been possible to find any relation between these AC fields and other variations in local ionospheric properties. This may, however, be more from the sensitivity and resolution of the measurements being correlated with, rather than a real lack of connection with variations in plasms parameters.

TYPE C IRREGULARITIES - "RISING SPECTRUM" IRREGULARITIES - EQUATORIAL HISS

The Type C irregularities, characterized by an amplitude spectrum with a positive slope in the frequency range 100 - 1000 Hz (λ 80-8m), i.e. $A \propto f^{+n}$, $n > 0$, will have typical amplitudes of 0.5 - 1 $\mu Vm^{-1}Hz^{-\frac{1}{2}}$ at 500 Hz. They are considerably weaker in total amplitude than the Type A fields, but their high frequency (short wavelength) components are much stronger. The Type C events usually appear at the equator ($\pm 5^{\circ}$).

No connection is found between spread F and Type C irregularities (cf. Figures 9 and 10), a fact which is not very surprising when one considers the wavelengths of these electric field structures and the resolution and spatial sensitivity range of a HF ionosonde. Within the sensitivity limits of the DC electric field instrumentation it has not been possible to see any variations in the DC field directly related to the Type C variations. The spatial resolution of the plasma composition experiments precludes detection of ionization microstructures which may be related to the field fluctuations.

On a larger scale, the Type C fields have been seen in regions where large depletions in ionization, "holes" in total ion concentration

(Hanson and Sanatani, 1973), appeared. Such an example is shown in Figure 14. A Type A field is found on the gradients at each side of the "hole", while the Type C occurs in the bottom of the "hole". The connection between these large depressions of ionization and the small scale AC fields is not yet clear, and is presently under more thorough examination. A preliminary conclusion seems to be that Type C fields appear when "holes" in ionization are seen near the equator (a reversal of this relation will not necessarily be valid).

The presence of AC electric fields at VLF frequencies at the equator has previously been reported by Laaspere et al. (1971; 1974). From the examples of this "equatorial hiss" published in the literature, a connection seems to exist between the Type C fields and the hiss, and it seems tempting to conclude that they really are observations of the same phenomenon. The differences which do appear can be ascribed to differences in sensitivity and frequency range.

DISCUSSION

Several other observations, while not directly comparable to the OGO 6 electric field data, almost certainly involve similar processes. Reported irregularity spectra from radio scintillation observations (e.g. Elkins and Papagiannis, 1969; Whitney and Cantor, 1975) as well as *in situ* observations of electric fields (Kelley and Mozer, 1972) and structures in ionization (Dyson et al., 1974; Sagalyn et al. 1975) all exhibit a frequency dependence where the amplitude peaks at low frequencies (or low k) and then follows a power law $f^{-1.2 \pm 0.3}$ similar to our Type A. The lack of observations that would correspond to our Types B and C is most likely

to be an effect of their sensitivity rather than a real absence of smaller scale irregularities. The presence of 3 m irregularities (~ 2.7 kHz in our Doppler shifted frequency representation) has indeed been shown to be a rather common feature in the nighttime F region by numerous VHF radar observations (e.g. Farley et al., 1970). These observations also distinguish between "strong irregularities", observed when spread F was detected by HF ionosondes, and weak irregularities, when spread F could not be seen on the ionograms. A possible conclusion is that the strong events are related to our Type A, while the weak irregularities are associated with Type B and/or C. More complex spectra, including peaks in a power law background spectrum, have also been proposed by Wernik and Liu (1974) to explain observed features in radio scintillation at GHz frequencies. However, the bulk of the data obtained on equatorial F-region irregularities, by ground based radio techniques and topside sounding, and by in situ plasma probe measurements, undoubtedly represent measurements which most readily can be related to our strong Type A variational fields, or the "classical" spread F irregularities.

A multitude of theories for generation of spread F irregularities have been advanced (cf. e.g. Herman, 1966 for a review of spread F, observations and theory). The main types of mechanisms can, however, basically be regarded as members of one or more of the following families:

I: Amplification of irregularities in ionization by vertical motion in the presence of gradients (Martyn, 1959; Calvert, 1963; Simon, 1963)

II: Gravitational, Rayleigh-Taylor, instability (Dungey, 1956;

III: Coupling and transfer of irregularities from the E to the F region

(Dagg, 1957; Cole, 1971); IV: Ionization irregularities produced by precipitating particles; and V: Coupling with hydromagnetic waves (Singleton, 1966).

Even though the observation of energetic particles at the equator reported by Heikkila (1971) has possibly brought up a new mechanism for equatorial spread F, it does not at present seem to be the major source. Spread F is a very common phenomenon, while these equatorial particle events seem, at least from the existing observations, to be rather scattered. It seems unlikely that they can account for the majority of the irregularity observations.

Mechanisms involving coupling between the E and F regions by equipotential magnetic field lines, in which one can avoid some of the difficulties appearing when only considering the F region, have generally not been considered as prime candidates. The high attenuation in the propagation of small scale electric fields is one of the main reasons for this (Farley, 1960; Spreiter and Briggs, 1961). It would also be difficult, with these mechanisms, to account for separate layers of spread F structures which have been observed (Farley, et al., 1970) and for the multiple irregularity structures seen in the present data.

Farley et al., (1970) also examined the various theories which appear under the two first classes of generation mechanisms, and concluded that none of these could account for all the features in the radar observations of F region irregularities. A fundamental objection against existing theories was also that none of them could explain irregularities smaller than the ion Larmor radius, while the radar detection of 3 m structures

showed the presence of such dimensions in the irregularity spectrum. This short wavelength cut-off may, however, be eliminated by collisional diffusion (Rosenbluth et al., 1962).

It is, however, an open question whether the radar observed 3 m irregularities always occur as a part of strong long wavelength structures. Farley et al.'s distinction between weak and strong irregularities may indicate that this is not always so. Recent measurements of irregularities made simultaneously with a rocket borne plasma probe and ground based radar also give evidence for this (Kelley and Mozer, 1975). Our observations of different spectra in the equatorial F region show that 3 m structures can appear independeltly of strong long wavelength fields, and suggest that different mechanisms are probably involved in the generation of the different types of irregularities. Thus, the theories for strong spread F irregularities (or Type A events) may not necessarily have to satisfy all the conditions set by the radar data. The weak radar echoes may in fact be associated with Type B and C events.

Recent theoretical treatment of equatorial spread F has brought new life into the Rayleigh-Taylor instability. Dungey's early version of this mechanism (Dungey, 1956) has been further elaborated by Haerendel (Balsley et al, 1972; Haerendel, 1974) and by Hudson and Kennel (1975). It is shown that this instability mode can grow below the F peak, and produce irregularities which have many of the characteristics observed in spread F. However, the geometry in their models extends over whole flux tubes, and it is again, considering the observations of the highly structured Type A irregularity regions, difficult to see how a mechanism

operating over whole field line dimensions could produce such variations in space as seen in the Type A events. The amplitude variations with latitude seen in the Type B events, could, however, more resemble what one might expect from such a large scale geometry.

Our Observations of Type A irregularities, correlated with DC electric fields and/or ionization gradients, point more in the direction of a gradient instability as a source for the irregularities. Such instabilities have been examined by several workers (e.g., Cunnold, 1969), and recently by Hudson and Kennel (1975). Hudson and Kennel conclude that gradient driven modes can also be destabilized solely by the plasma density gradient, and that no destabilizing force ($\underline{E}$ or $\underline{g}$) is necessary. The mechanism will work both on the bottomside and the topside of the F peak. Gradient driven instabilities will also be more localized on the density gradient, which also is in agreement with our observations.

ACKNOWLEDGEMENT

The authors wish to thank the following persons for making non-published data available: Drs. W. B. Hanson and J. P. McClure, University of Texas at Dallas, and Dr. H. A. Taylor, Goddard Space Flight Center (plasma measurements), and Dr. E. J. Smith, Jet Propulsion Laboratory, California (search coil data). Ionosonde data used in connection with this article were obtained from WDC-A for Ionospheric Phenomena. One of the authors (J. A. H.) is indebted to the National Academy of Sciences - National Research Council for sponsoring his NAS-NRC Research Associateship at the Goddard Space Flight Center.

REFERENCES

Aggson, T. L., Probe measurements of electric fields in space, in Atmospheric Emissions, ed. B. M. McCormac and A. Omholt, Van Nostrand Reinhold Publ. Corp., N. Y., 305, 1969.

Balsley, B. B., G. Haerendel, and R. A. Greenwald, Equatorial spread F: Recent observations and a new interpretation, J. Geophys. Res., 77, 5625, 1972.

Booker, H. G., and H. W. Wells, Scattering of radio waves by the F region of the ionosphere, Terr. Magn., 43, 249, 1938.

Calvert W., Instability of the equatorial F layer after sunset, J. Geophys. Res., 68, 2591, 1963.

Cole, K. D., Formation of field-aligned irregularities in the magnetosphere, J. Atmos. Terr. Phys., 33, 741, 1971.

Cunnold, D. M., Drift-dissipative plasma instability and equatorial spread F, J. Geophys. Res., 74, 5709, 1969.

Dagg, M., The origin of ionospheric irregularities responsible for radio-star scintillations and spread F, 2, Turbulent motion in the dynamo region, J. Atmos. Terr. Phys., 11, 139, 1957.

Dungey, J. W., Convective diffusion in the equatorial F region, J. Atmos. Terr. Phys., 9, 304, 1956.

Dyson, P. L., J. P. McClure, and W. B. Hanson, In situ measurements of the spectral characteristics of F region ionospheric irregularities, J. Geophys. Res., 79, 1497, 1974.

Elkins, T. J., and M. D. Papagiannis, Measurements and interpretation of power spectrum of ionospheric scintillation at sub-auroral locations, J. Geophys. Res., 74, 4105, 1969.

Farley, D. T., A theory of electrostatic fields in the ionosphere at non-polar geomagnetic latitudes, J. Geophys. Res., 65, 869, 1960.

Farley, D. T., B. B. Balsley, R. F. Woodman, and J. P. McClure, Equatorial spread F: Implications of VHF radar observations, J. Geophys. Res., 75, 7199, 1970.

Haerendel, G., Theory of equatorial spread F, Preprint, Max-Planck-Institut für Physik and Astrophysik, 1974.

Hanson, W. B., and S. Sanatani, Large N_i gradients below the equatorial F peak, J. Geophys. Res., 78, 1167, 1973.

Hanson, W. B., S. Sanatani, D. Zuccaro, and T. W. Flowerday, Plasma measurements with the retarding potential analyzer on OGO 6, J. Geophys. Res., 75, 5483, 1970.

Heikkila, W. J., Soft particle fluxes near the equator, J. Geophys. Res., 76, 1076, 1971.

Herman, J. R., Spread F and ionospheric F-region irregularities, Rev. Geophys., 4, 255, 1966.

Heppner, J. P., Magnetospheric convection patterns inferred from high latitude activity, in Atmospheric Emissions, ed. by B. M. McCormac and A. Omholt. Van Nostrand Reinhold Publ. Corp., New York, 251, 1969.

Heppner, J. P., Electric field variations during substorms, Planet. Space Sci., 20, 1475, 1972.

Hudson, M. K., and C. F. Kennel, Linear theory of equatorial spread F, J. Geophys. Res., 80, 4581, 1975.

Kelley, M. C., and F. S. Mozer, A satellite survey of vector electric fields in the ionosphere at frequencies of 10 to 500 Hertz. 3. Low frequency equatorial emissions and their relationship to ionospheric turbulence, J. Geophys. Res., 77, 4183, 1972.

Kelley, M. C., and F. S. Mozer, A review of the recent results of in situ ionospheric irregularity measurements and their relation to electrostatic instabilities, Paper 1-5 in Proceedings from the Symposium on the Effects of the Ionosphere on Space Systems and Communications, Naval Research Laboratory, Washington, D. C., 1975.

Laaspere, T., and W. C. Johnson, Additional results from an OGO 6 experiment concerning ionospheric electric and electromagnetic fields in the range 20 Hz to 540 kHz, J. Geophys. Res., 78, 2926, 1973.

Laaspere, T., and L. C. Semprebon, The global distribution of natural and man-made ionospheric electric fields at 200 kHz and 540 kHz as observed by OGO 6, J. Geophys. Res., 79, 2393, 1974.

Laaspere, T., W. C. Johnson, and L. C. Semprebon, Observations of auroral hiss, LHR noise, and other phenomena in the frequency range 20 Hz to 540 kHz on OGO 6, J. Geophys. Res., 76, 4477, 1971.

Martyn, D. F., Large-scale movements of ionization in the ionosphere, J. Geophys. Res., 64, 2178, 1959.

Maynard, N. C., Electric field measurements across the Harang discontinuity, J. Geophys. Res., 79, 4620, 1974.

Maynard, N. C., and J. P. Heppner, Variations in electric fields from polar orbiting satellites, in Particles and Fields in the Magnetosphere, ed. by B. M. McCormac, D. Reidel Publ. Corp., Dordrecht, Holland, 247, 1970.

Muzzio, J. L. R., and J. J. Angerami, OGO 6 observations of extremely low frequency hiss, J. Geophys. Res., 77, 1157, 1972.

Piggott, W. R., and K. Rawer (Eds.), U.R.S.I. Handbook of ionogram interpretation and reduction (2. edition), Report UAG-23, World Data Center A for Solar-Terrestrial Physics, NOAA, Boulder, Colorado, 1972.

Rosenbluth, M. N., N. Krall, and N. Rostoker, Finite Larmor radium stabilization of weakly unstable confined plasmas, Nuclear Fusion Supplement, 1, 143, 1962.

Sagalyn, R. C., A. D. R. Phelps, and M. Ahmed, In situ measurements of the structure and spectral characteristics of small scale F region ionospheric irregularities, Paper 6-10 in Proceedings from the Symposium on the Effects of the Ionosphere on Space Systems and Communications, Naval Research Laboratory, Washington, D. C., 1975.

Simon, A., Instability of a partially ionized plasma in crossed electric and magnetic fields, Phys. Fluids, 6, 382, 1963.

Singleton, D. G., The production of spread F irregularities, in Spread F and its Effects upon Radiowave Propagation and Communication, ed. P. Newman, Agardograph 95, Technivision, Maidenhead, UK, 553, 1966.

Spreiter, J. R., and B. R. Briggs, Theory of electrostatic fields in the ionosphere at polar and middle geomagnetic latitudes, J. Geophys. Res., 66, 1731, 1961.

Taylor, W. W. L., and D. A. Gurnett, Morphology of VLF emissions observed with the Injun 3 satellite, J. Geophys. Res., 73, 5615, 1968.

Wernik, A. W., and C. H. Liu, Ionospheric irregularities causing scintillation of GHz frequency radio signals, J. Atmos. Terr. Phys., 36, 871, 1974.

Whitney, H. E. and C. Cantor, Amplitude and fade statistics for equatorial scintillations, Paper 2-3 in Proceedings from the symposium on the Effects of the Ionosphere on Space Systems and Communications, Naval Research Laboratory, Washington, D. C., 1975.

FIGURE CAPTIONS

Figure 1A: Electric field amplitude variations measured on the dusk side, magnetic local times ~ 1800, in a pass going from dip latitude - 15° and into the northern polar cap. The upper panel gives the DC field, with the $\underline{v} \times \underline{B}$ component subtracted. The five lower panels show the AC amplitude within the frequency bands noted on the figure.

Figure 1B: This figure is a continuation of the pass shown in Figure 1A, and shows the DC and AC electric field variations on the dawn side, magnetic local time ~ 0545, going from the northern polar cap to dip latitude - 11°.

Figure 2: Amplitude spectra of the AC electric fields measured inside the polar cap (dotted line) altitude ~ 625 km, the auroral oval (dash-dot), altitude ~ 500 km, and the subauroral belt (dashes), altitude ~ 425 km. The data points are all 30 s averages. The fully drawn line represents the amplifier noise level.

Figure 3: Amplitude variations in DC and AC electric field recorded by the satellite in a dawn side pass going from the northern polar cap, through the equatorial region, to - 24° dip latitude. The enhanced AC field seen around the equator, is what is referred to as a Type A irregularity.

Figure 4: Typical amplitude vs. frequency spectra of the fields in the Type A irregularity. The four spectra are taken from different sectors of an irregularity region in the same satellite pass. The data points are 30 s averages.

Figure 5: Electric field record showing a pass with a Type B equatorial irregularity. Compared to the Type A, shown in Figures 1B and 3, the Type B irregularity is much weaker, but it contains more power in the highest frequencies.

Figure 6: Typical amplitude spectra of a Type B irregularity. The data are from the pass shown in Figure 13.

Figure 7: The left hand side of the figure shows the AC fields in a Type C irregularity, and the right hand side amplitude spectra from two different portions of the pass. A weak Type A field is mixed with the Type C and causes a somewhat increased level in the 4-16 Hz channel, mainly on both sides of the peak seen in the 256-1024 Hz channel. The main characteristic of the Type C noise, the rising spectrum, is, however, prominent.

Figure 8: Plot showing distribution of Type A irregularities as function of altitude and L-value. Heavy orbit lines are used to indicate the presence of irregularities. The lightly drawn sections represent the low latitude parts of the passes without irregularities. The end of the orbit lines will in each case show the high latitude end of the irregularities. A short, light line is used as a symbol for passes without Type A fields. The data used for this figure are from the period October 7 to November 22, 1969. All passes took place in the geographic longitude sector 100°W to 30°E, and only periods with low magnetic activity have been used.

Figure 9: Orbit plots for succeeding dawnside passes of OGO 6. Amplitude variations recorded in the 4-16 Hz and 64-256 Hz channels are shown on the right and left hand side of the orbit line, respectively. (Only parts where the signal exceeds the amplifier noise level are shown.) Information about spread F activity, as observed by ground based ionosondes, are also included. Hourly values of foF2 have been used. The coding is the following: triangles represent stations where spread F was observed in the hour interval when the satellite pass took place, circles are stations without spread F. (For station identification cf. Piggott and Rawer, 1972). The bars across the orbit lines show the low latitude boundary of the sub auroral AC electric fields. Dotted lines represent data gaps. The dip equator is drawn as a heavy line across the map.

Figure 10: Plots of succeeding low latitude passes by OGO 6 on the nightside. Amplitude variations in the electric field within the bands 4-16 Hz and 256-1024 Hz are shown on the right and left hand side of the orbit line, respectively. Spread F actively detected by ground based ionosondes is also indicated. Hourly values of foF2 are used, and the coding is the following: a triangle represents a station where spread F was observed in the hour interval when the satellite pass took place, a circle represents a station without spread F. (For station identification cf. Piggott and Rawer, 1972.) The bars across the orbit lines show the low latitude boundary of the sub auroral AC fields. Dotted orbit lines represent data gaps.

Figure 11: Type A irregularities and variations in the local plasma. In the lower panel a Type A irregularity region is represented by the variations recorded in the 4-16 Hz band. The upper panel shows variations in the local plasma composition and fluctuations in ionization, $\Delta N_i/N_i$. (The plasma measurements are from the retarding potential analyzer in OGO 6, and are kindly provided by Dr. W. B. Hanson, University of Texas at Dallas.)

Figure 12: Type A irregularities detected by the electric field experiment and simultaneous observations of ionization irregularities seen by the retarding potential analyzer. (Magnetic local time for the equatorial crossing $\sim$ 2200.) (Plasma data are kindly provided by Dr. W. B. Hanson, University of Texas at Dallas.)

Figure 13: AC electric field variations and fluctuations in ionization observed in an equatorial pass in the morning sector (local magnetic time $\sim$ 0645). (Notice the difference from the typical nighttime events shown in Figures 11 and 12.) A region with ionization irregularities is observed between $\sim$ 0727 and 0734 UT without any accompanying electric field variations. Around the dip equator, however, Type B irregularities are seen in the electric field recordings, but no counterpart is here detected in the plasma measurements. (Plasma data are kindly provided by Dr. W. B. Hanson, University of Texas at Dallas.)

Figure 14: Variation in AC electric field (upper part) and ion concentration (lower part) observed in an equatorial crossing of OGO 6. Symbols represent the following: Squares, electron concentration; plus sign, ion mass $m_i^+ = 16$; crosses, $m_i^+ = 30$; and diamonds $m_i^+ = 56$. (Hanson and Sanatani, 1973). Large gradients in ionization and changes in ion composition are observed close to the dip equator. Type A electric field irregularities are present in the gradient regions, while Type C irregularities are seen in the N_i minimum region.

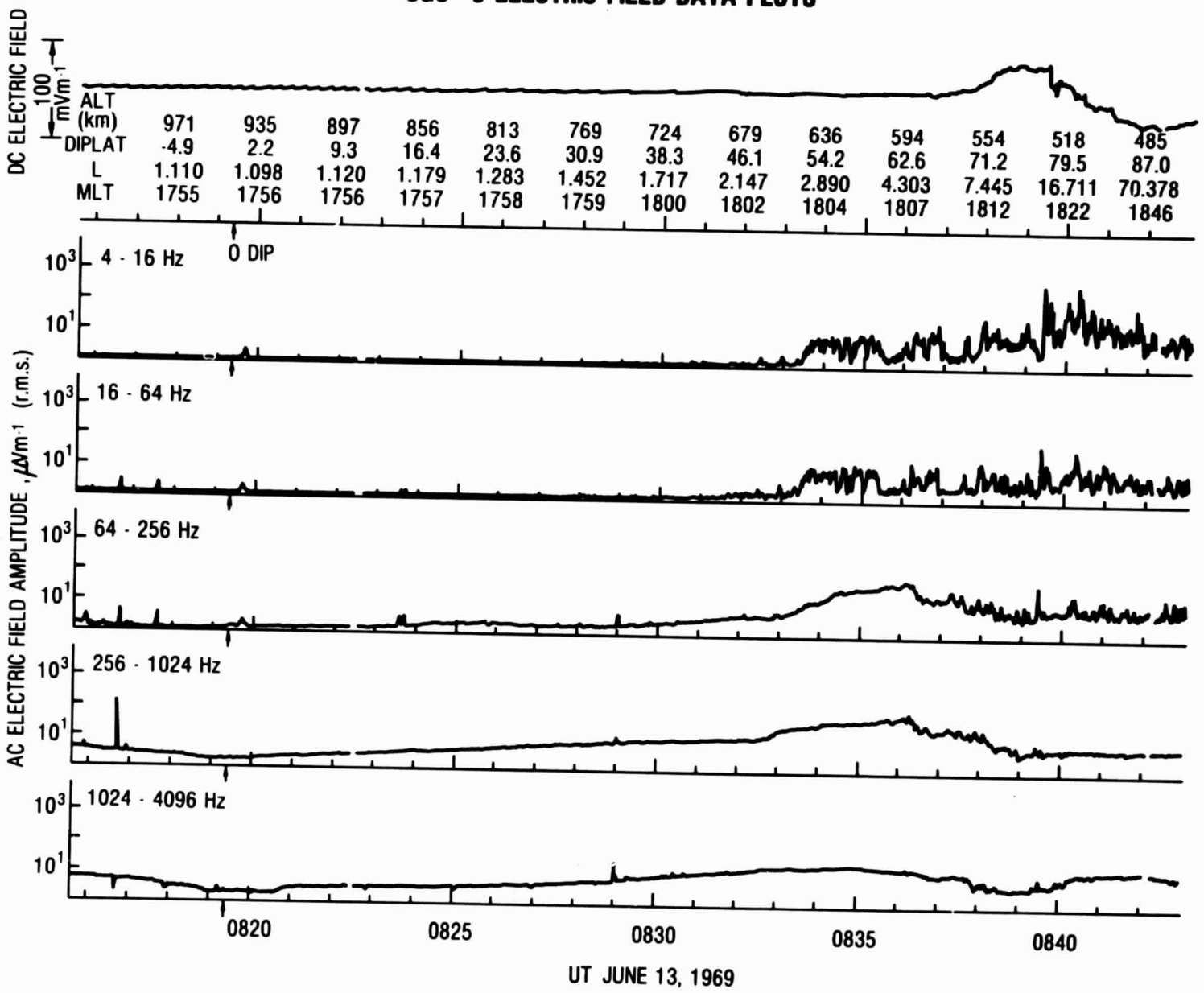
OGO--6 ELECTRIC FIELD DATA PLOTS
DC ELECTRIC FIELD
100 mVm⁻¹
ALT (km) 971 935 897 856 813 769 724 679 636 594 554 518 485
DIPLAT -4.9 2.2 9.3 16.4 23.6 30.9 38.3 46.1 54.2 62.6 71.2 79.5 87.0
L 1.110 1.098 1.120 1.179 1.283 1.452 1.717 2.147 2.890 4.303 7.445 16.711 70.378
MLT 1755 1756 1756 1757 1758 1759 1800 1802 1804 1807 1812 1822 1846
0 DIP
AC ELECTRIC FIELD AMPLITUDE, μVm⁻¹ (r.m.s.)
10³
10¹
4 - 16 Hz
16 - 64 Hz
64 - 256 Hz
256 - 1024 Hz
1024 - 4096 Hz
0820
0825
0830
0835
0840
UT JUNE 13, 1969

Figure 1A

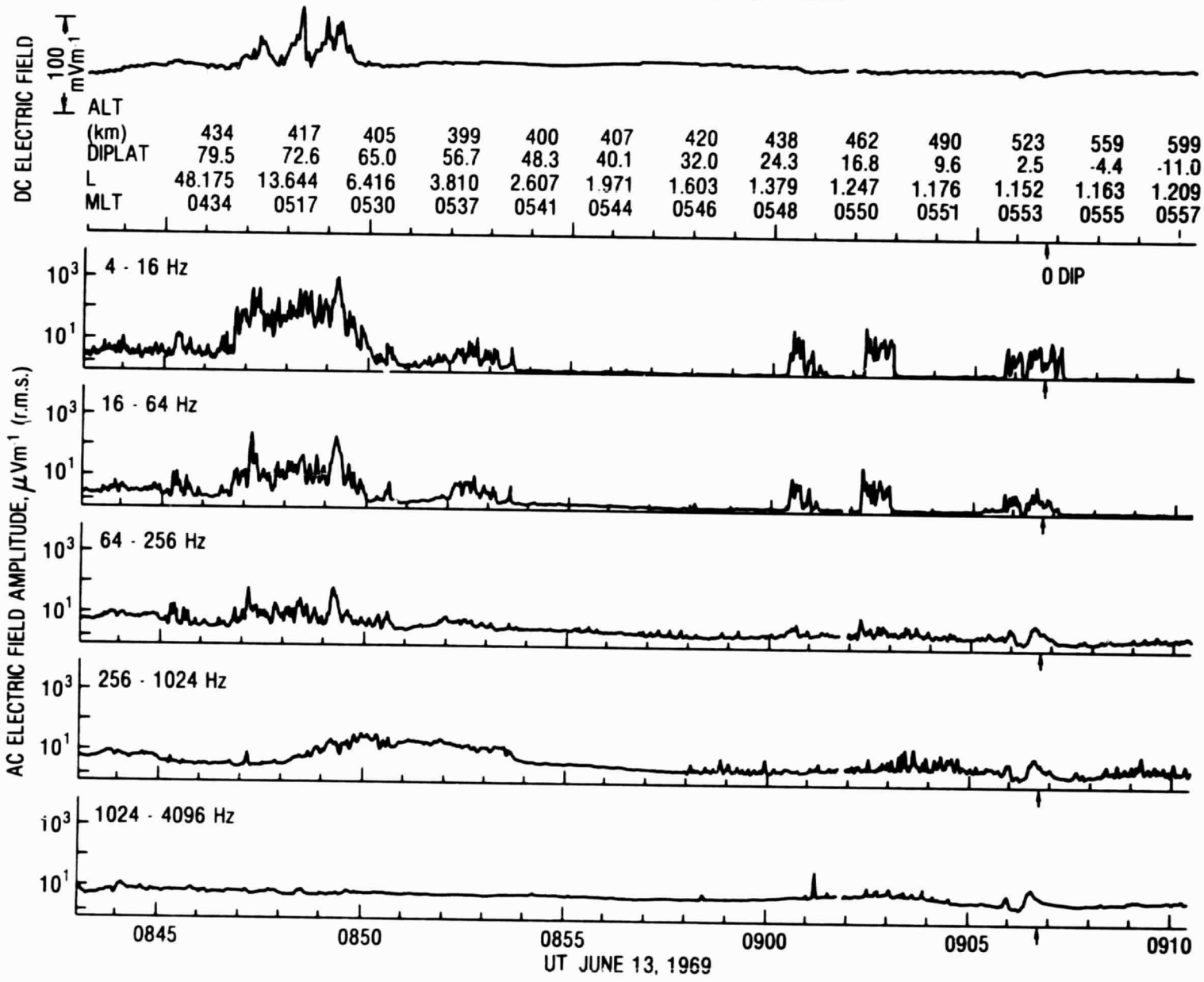
OGO—6 ELECTRIC FIELD DATA PLOTS
DC ELECTRIC FIELD
100 mVm⁻¹
ALT
(km) 434 417 405 399 400 407 420 438 462 490 523 559 599
DIPLAT 79.5 72.6 65.0 56.7 48.3 40.1 32.0 24.3 16.8 9.6 2.5 -4.4 -11.0
L 48.175 13.644 6.416 3.810 2.607 1.971 1.603 1.379 1.247 1.176 1.152 1.163 1.209
MLT 0434 0517 0530 0537 0541 0544 0546 0548 0550 0551 0553 0555 0557
0 DIP
AC ELECTRIC FIELD AMPLITUDE, μVm⁻¹ (r.m.s.)
4 - 16 Hz
16 - 64 Hz
64 - 256 Hz
256 - 1024 Hz
1024 - 4096 Hz
10³
10¹
0845 0850 0855 0900 0905 0910
UT JUNE 13, 1969

Figure 1B

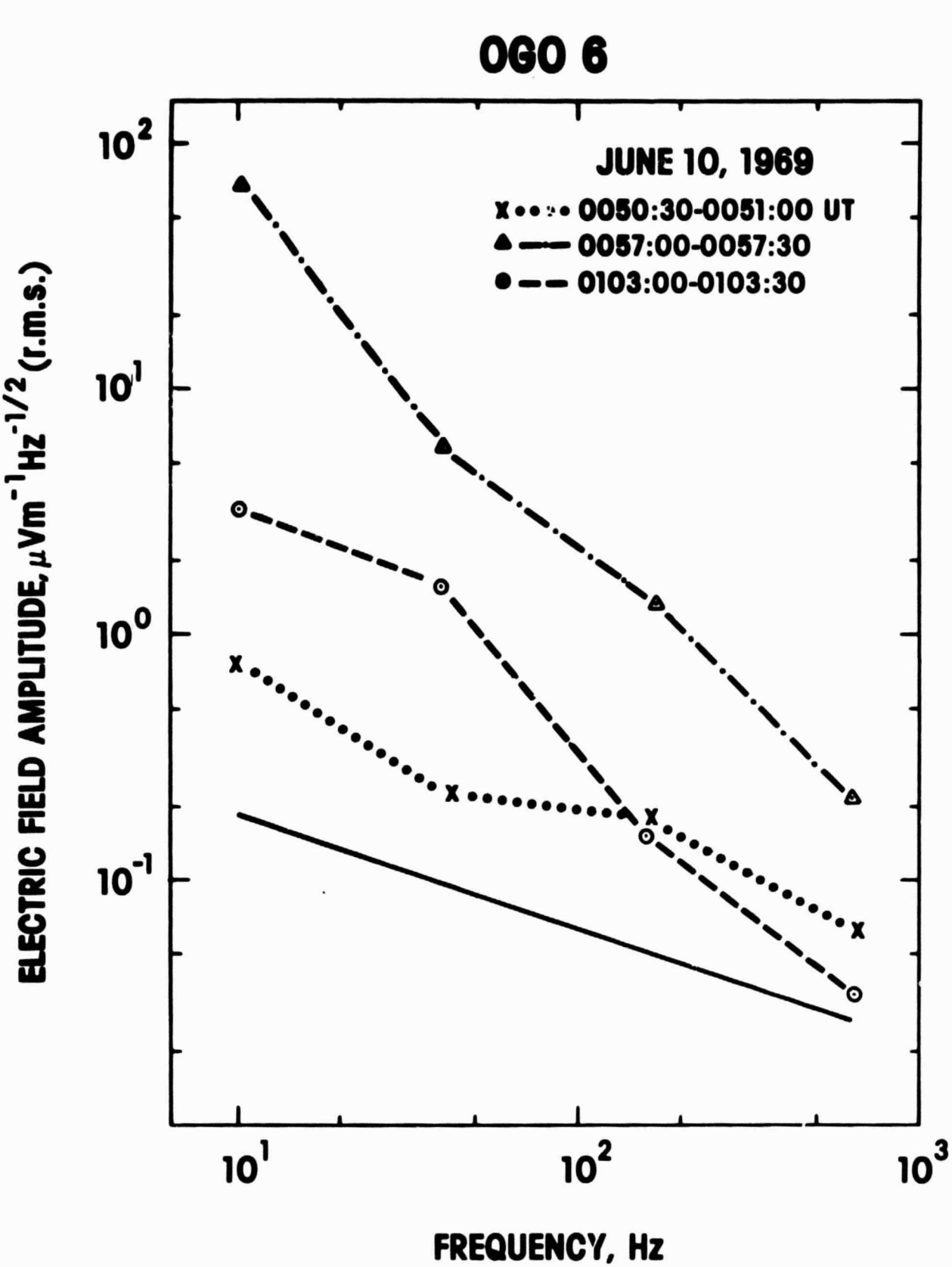
OGO 6
JUNE 10, 1969
0050:30-0051:00 UT
0057:00-0057:30
0103:00-0103:30
ELECTRIC FIELD AMPLITUDE, μVm⁻¹Hz⁻¹/²(r.m.s.)
FREQUENCY, Hz
10²
10¹
10⁰
10⁻¹
10¹
10²
10³

Figure 2

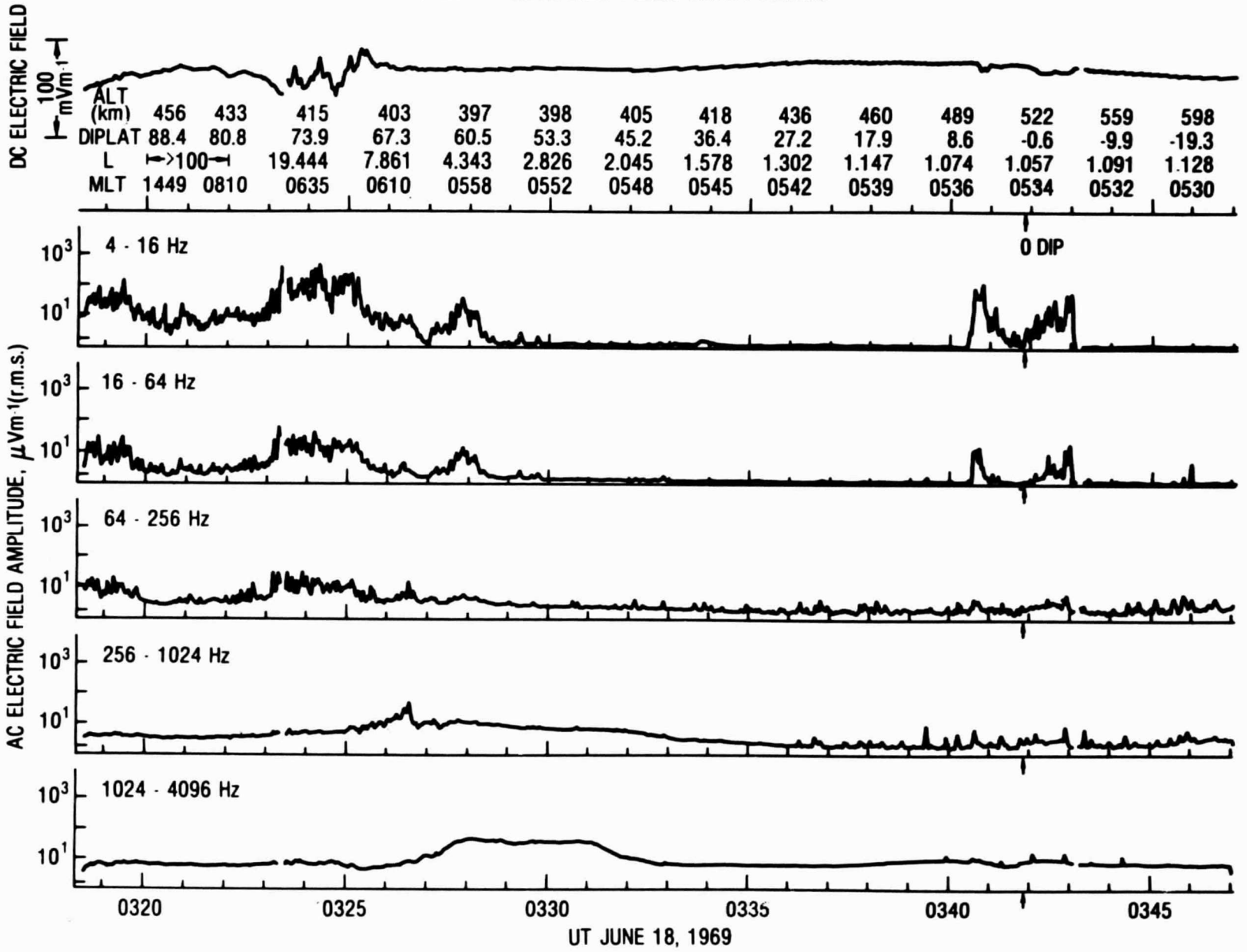
OGO–6 ELECTRIC FIELD DATA PLOTS
DC ELECTRIC FIELD
100 mVm⁻¹
ALT (km) 456 433 415 403 397 398 405 418 436 460 489 522 559 598
DIPLAT 88.4 80.8 73.9 67.3 60.5 53.3 45.2 36.4 27.2 17.9 8.6 -0.6 -9.9 -19.3
L ⟷100⟷ 19.444 7.861 4.343 2.826 2.045 1.578 1.302 1.147 1.074 1.057 1.091 1.128
MLT 1449 0810 0635 0610 0558 0552 0548 0545 0542 0539 0536 0534 0532 0530
0 DIP
AC ELECTRIC FIELD AMPLITUDE, μVm⁻¹(r.m.s.)
4 - 16 Hz
16 - 64 Hz
64 - 256 Hz
256 - 1024 Hz
1024 - 4096 Hz
10³
10¹
0320
0325
0330
0335
0340
0345
UT JUNE 18, 1969

Figure 3

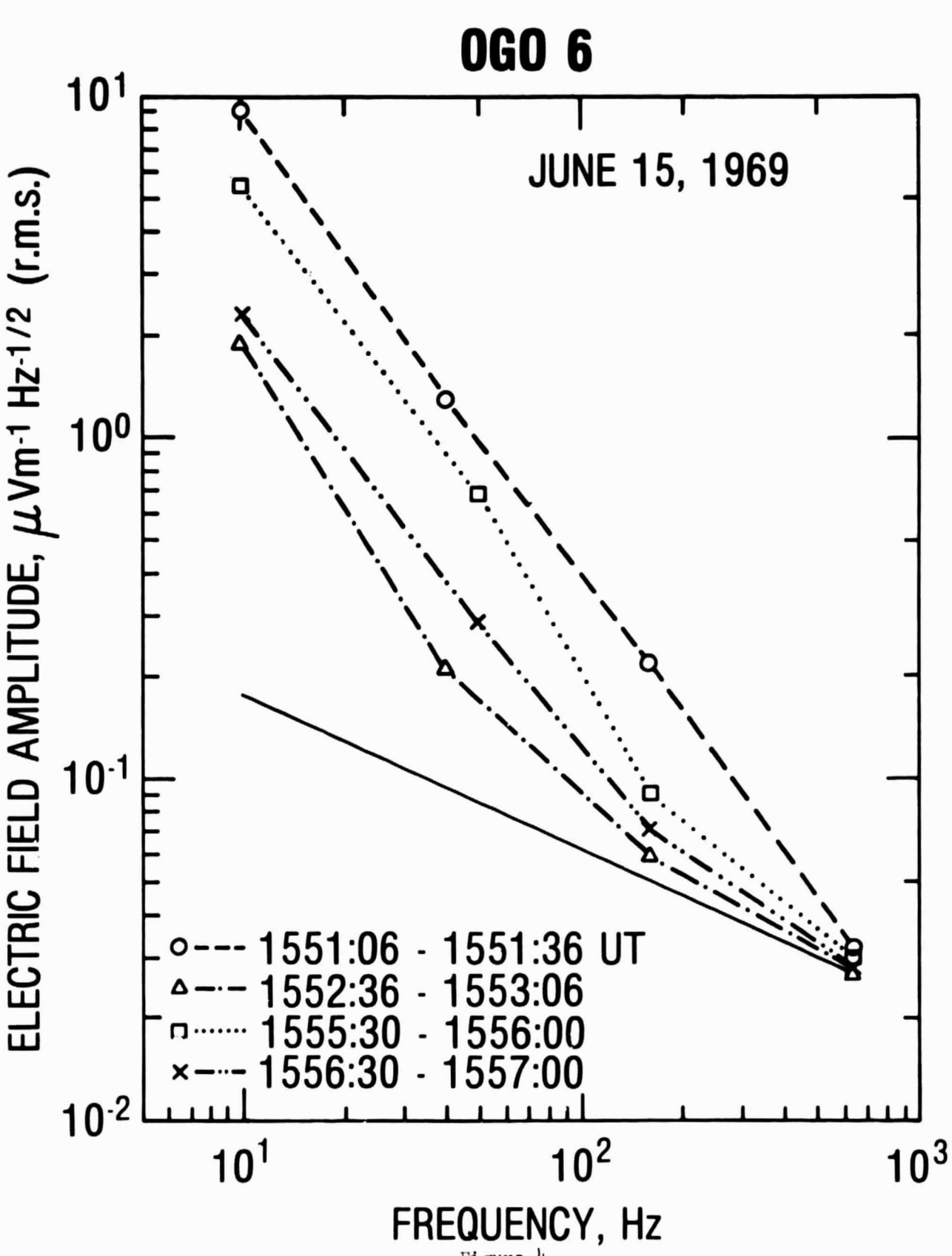
OGO 6
JUNE 15, 1969
ELECTRIC FIELD AMPLITUDE, μVm⁻¹ Hz⁻¹/² (r.m.s.)
10¹
10⁰
10⁻¹
10⁻²
10¹
10²
10³
FREQUENCY, Hz
1551:06 - 1551:36 UT
1552:36 - 1553:06
1555:30 - 1556:00
1556:30 - 1557:00

Figure 4

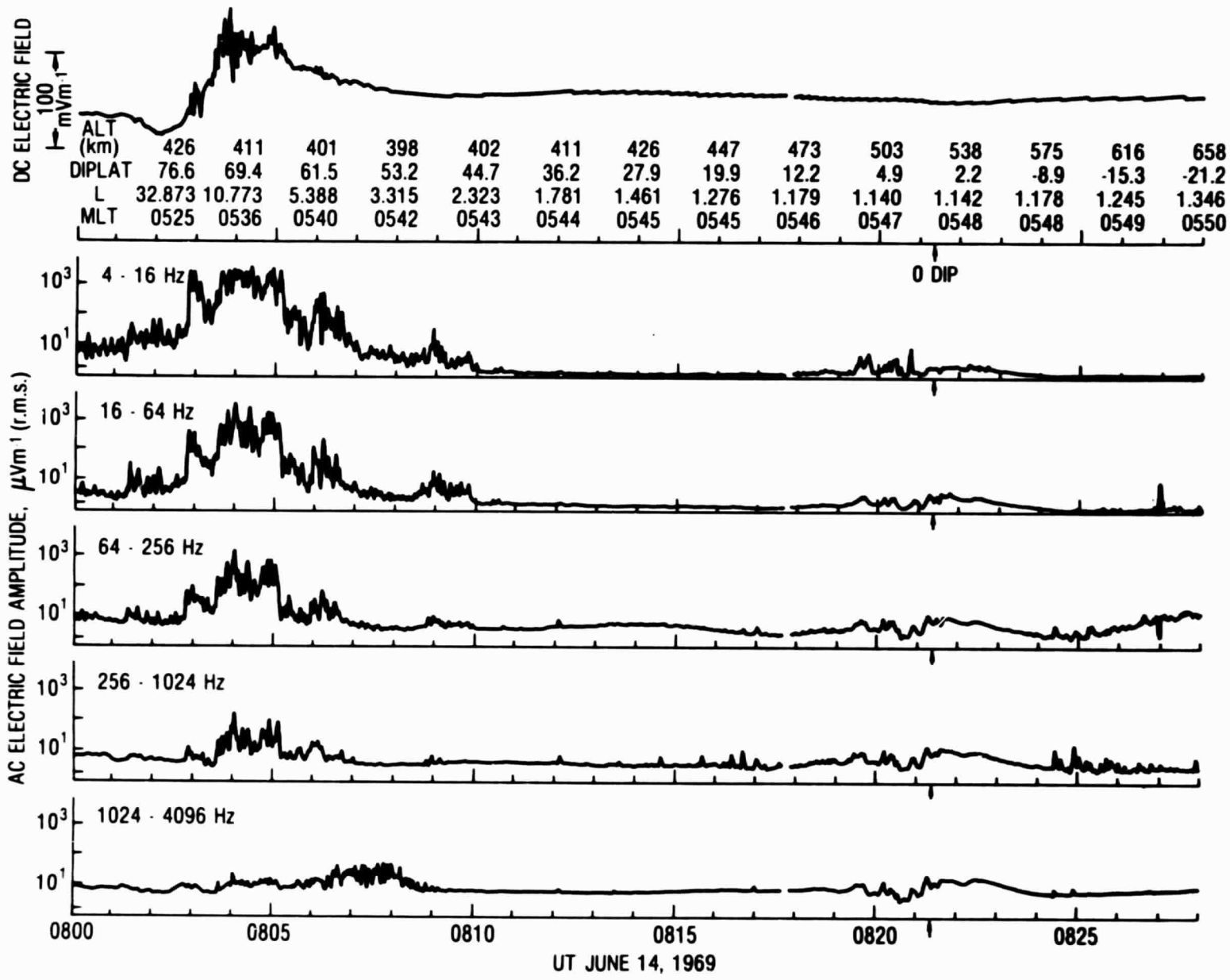
OGO–6 ELECTRIC FIELD DATA PLOTS
DC ELECTRIC FIELD
100 mVm⁻¹
ALT (km) 426 411 401 398 402 411 426 447 473 503 538 575 616 658
DIPLAT 76.6 69.4 61.5 53.2 44.7 36.2 27.9 19.9 12.2 4.9 2.2 -8.9 -15.3 -21.2
L 32.873 10.773 5.388 3.315 2.323 1.781 1.461 1.276 1.179 1.140 1.142 1.178 1.245 1.346
MLT 0525 0536 0540 0542 0543 0544 0545 0545 0546 0547 0548 0548 0549 0550
0 DIP
AC ELECTRIC FIELD AMPLITUDE, μVm⁻¹ (r.m.s.)
4 - 16 Hz
16 - 64 Hz
64 - 256 Hz
256 - 1024 Hz
1024 - 4096 Hz
10³
10¹
0800
0805
0810
0815
0820
0825
UT JUNE 14, 1969

Figure 5

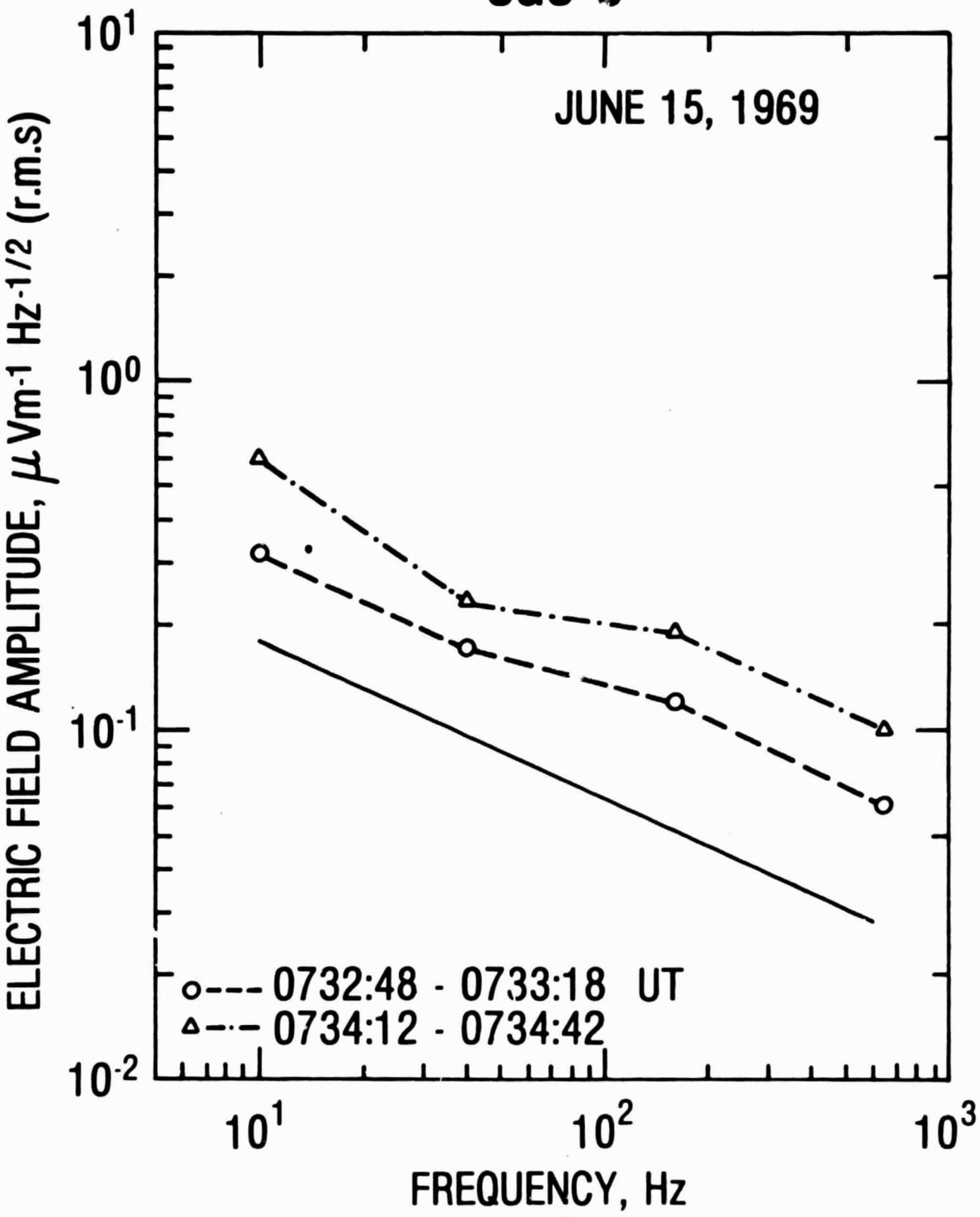
OGO 6
JUNE 15, 1969
ELECTRIC FIELD AMPLITUDE, μVm-1 Hz-1/2 (r.m.s)
10^1
10^0
10^-1
10^-2
10^1
10^2
10^3
FREQUENCY, Hz
0732:48 - 0733:18 UT
0734:12 - 0734:42

Figure 6

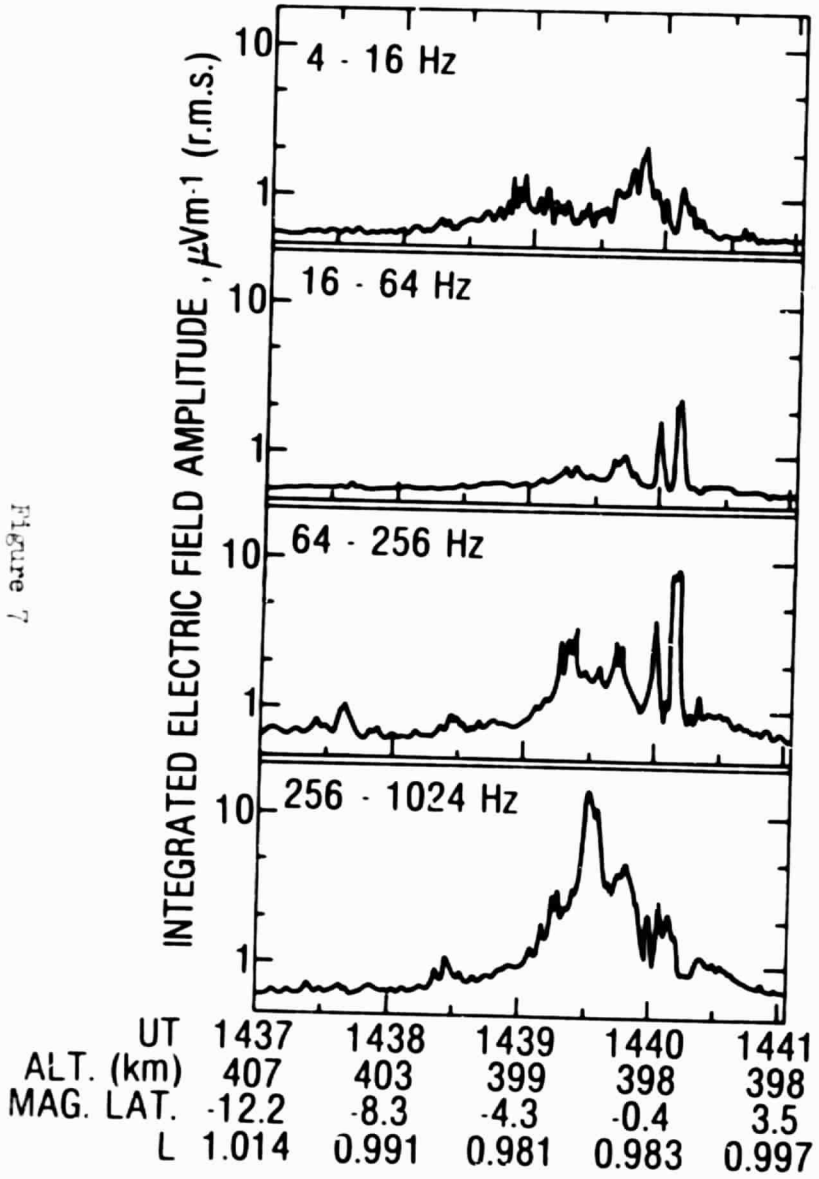

Figure 7

OGO 6

NOVEMBER 16 , 1969

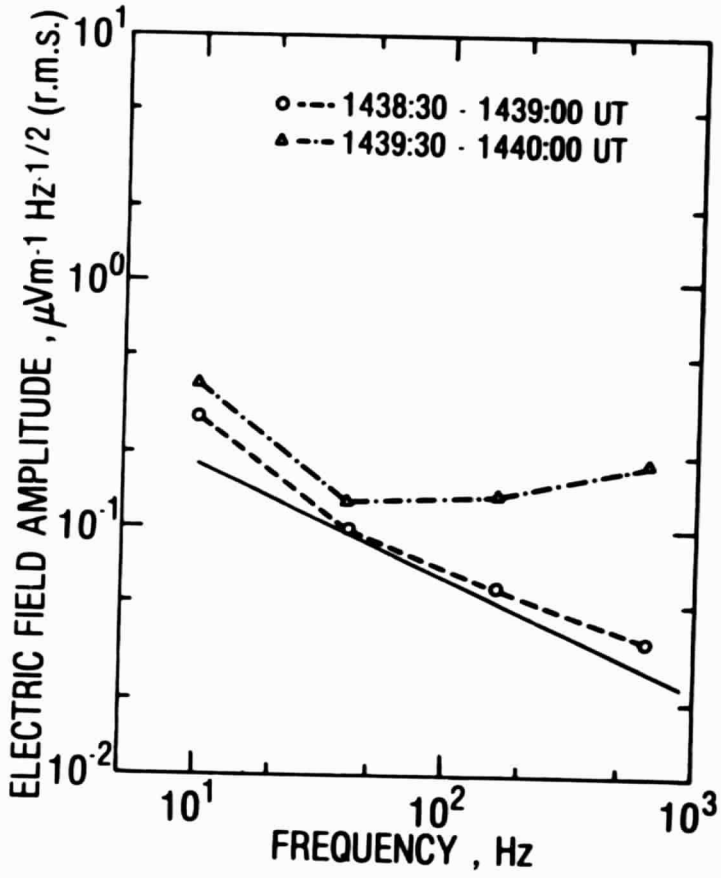

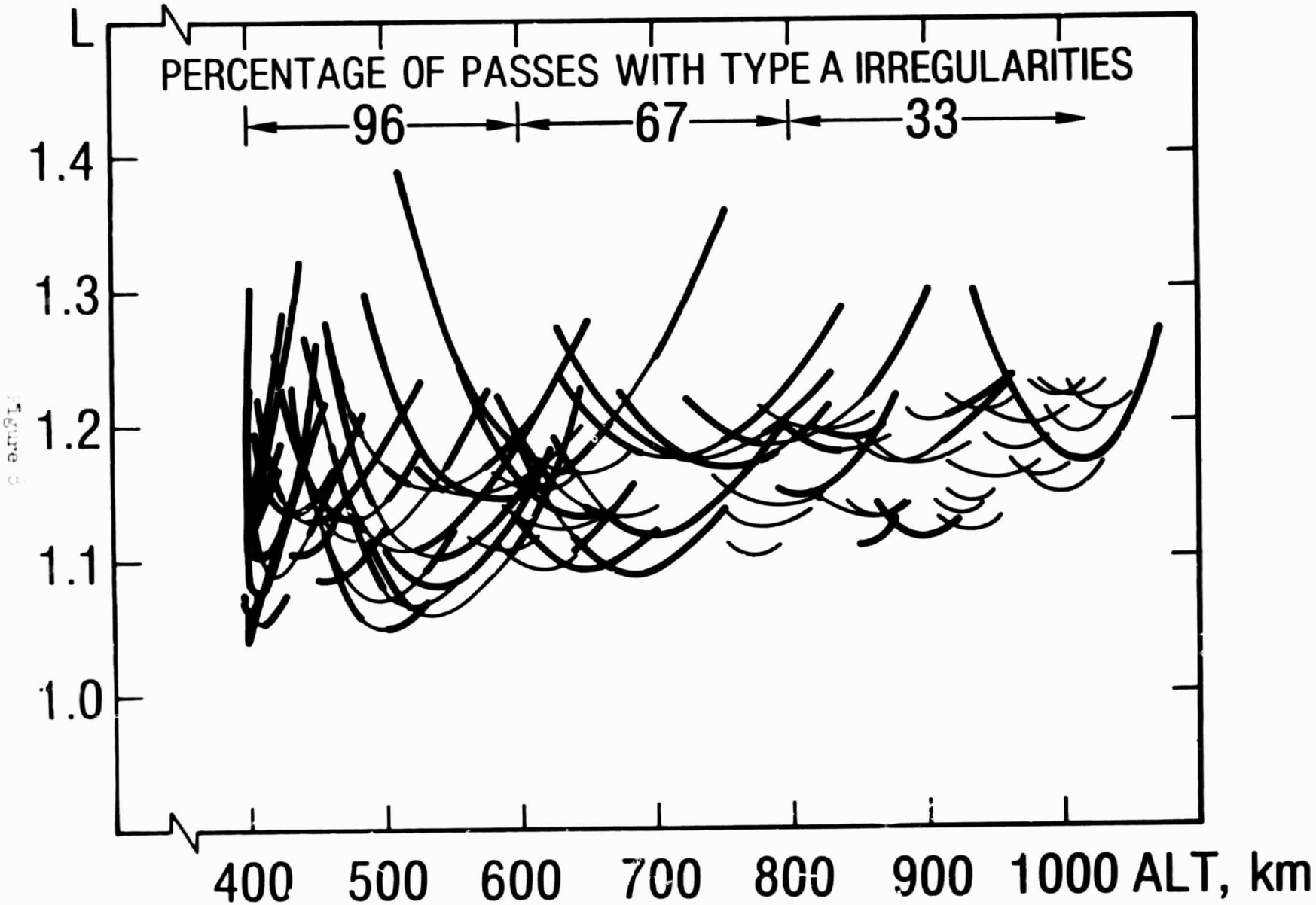
L
PERCENTAGE OF PASSES WITH TYPE A IRREGULARITIES
96
67
33
1.4
1.3
1.2
1.1
1.0
400
500
600
700
800
900
1000
ALT, km

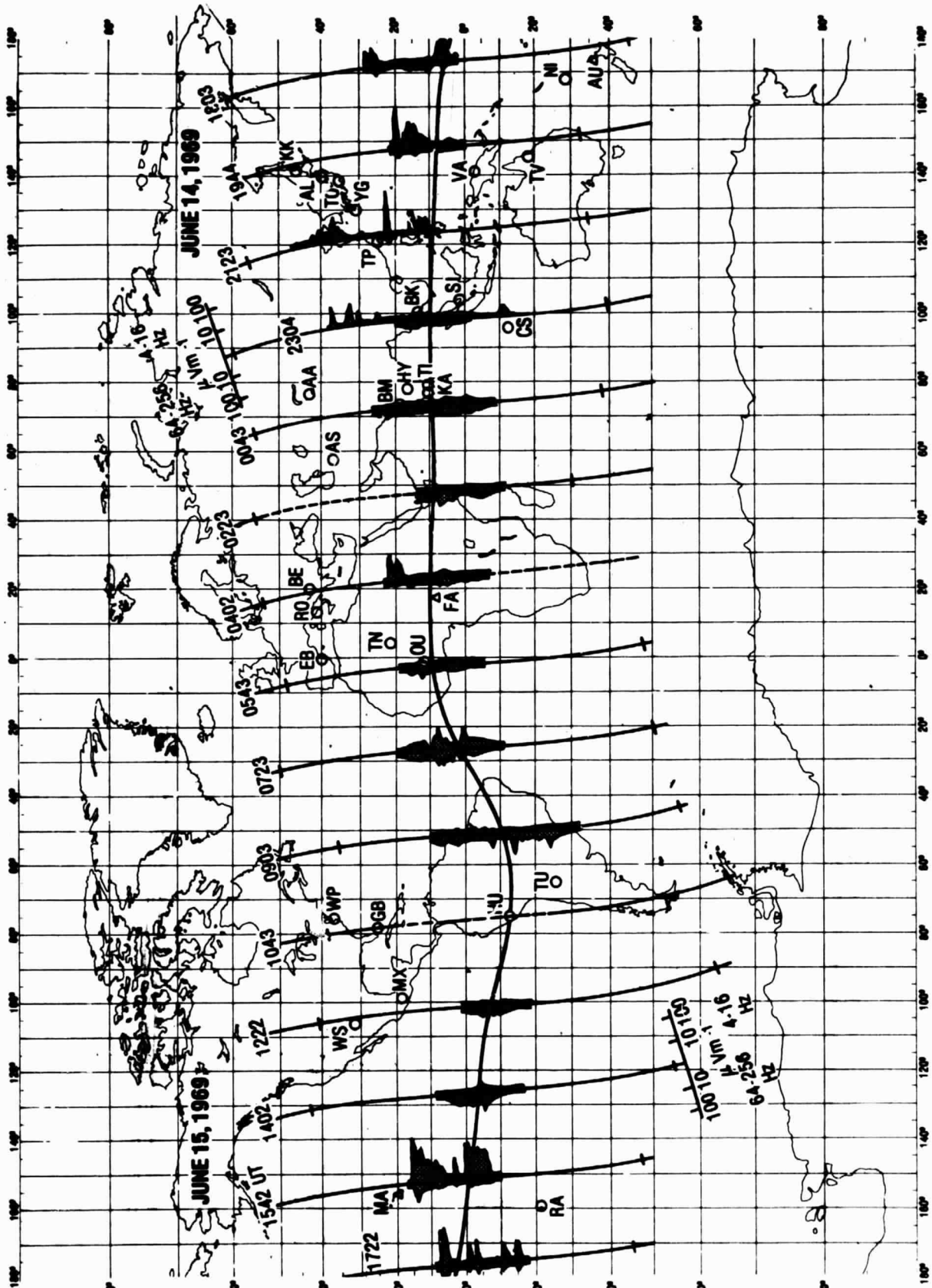

Figure 9

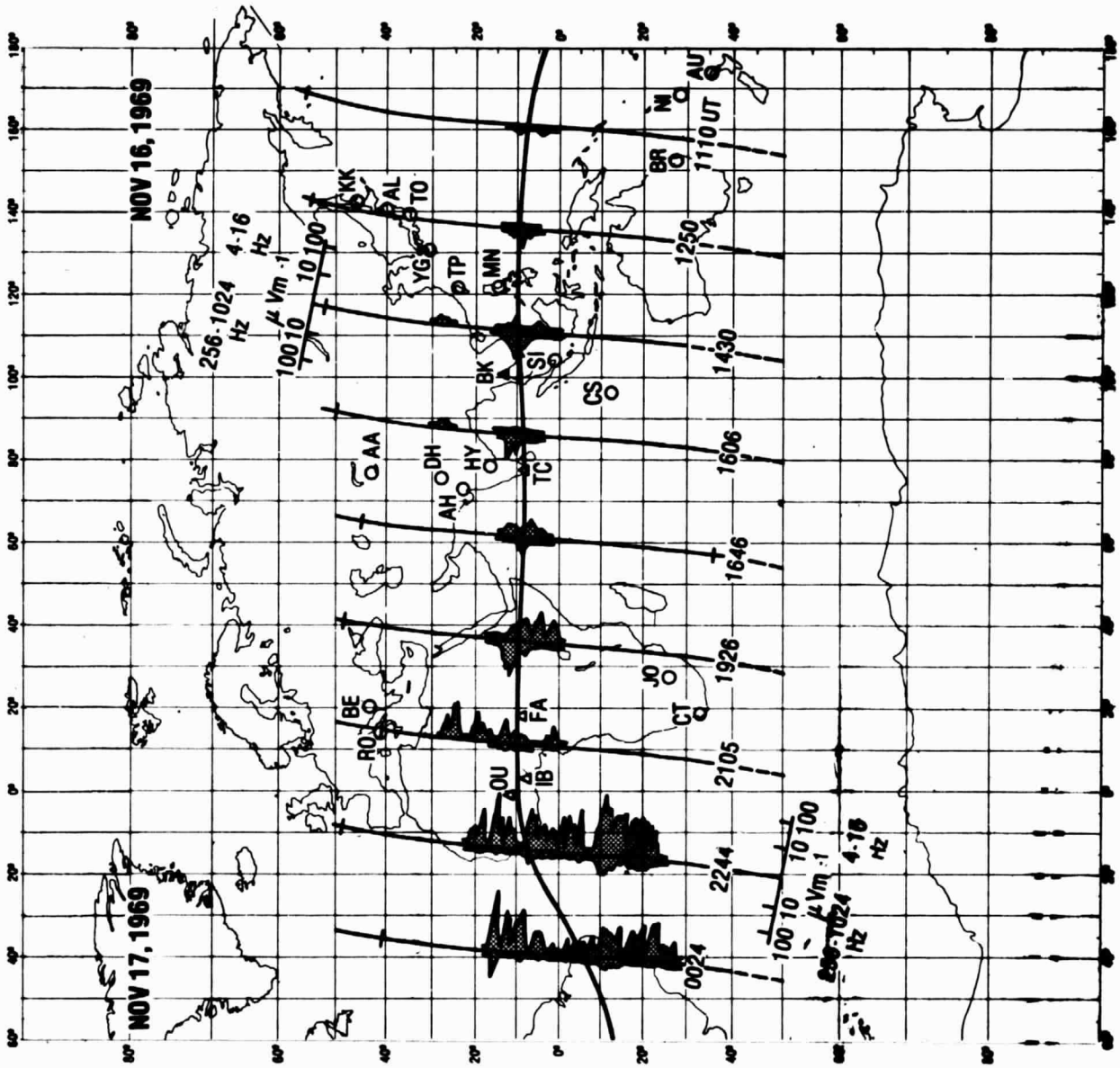

Figure 10

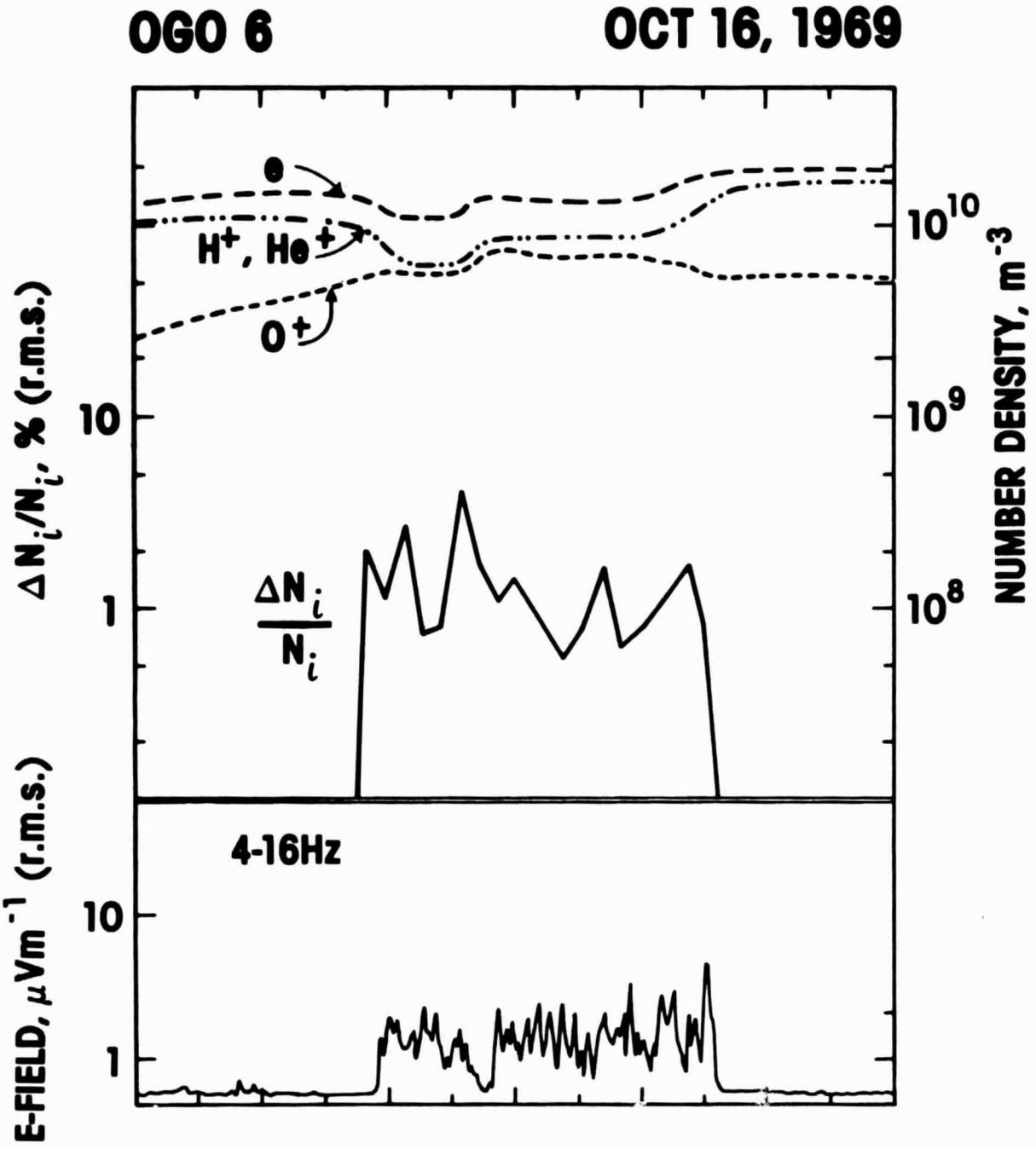

UT	0531	0533	0535	0537
ALT (km)	992	960	924	886
MAG. LAT.	-16.7	-10.1	-3.4	3.4
L	1.298	1.240	1.211	1.212

Figure 11

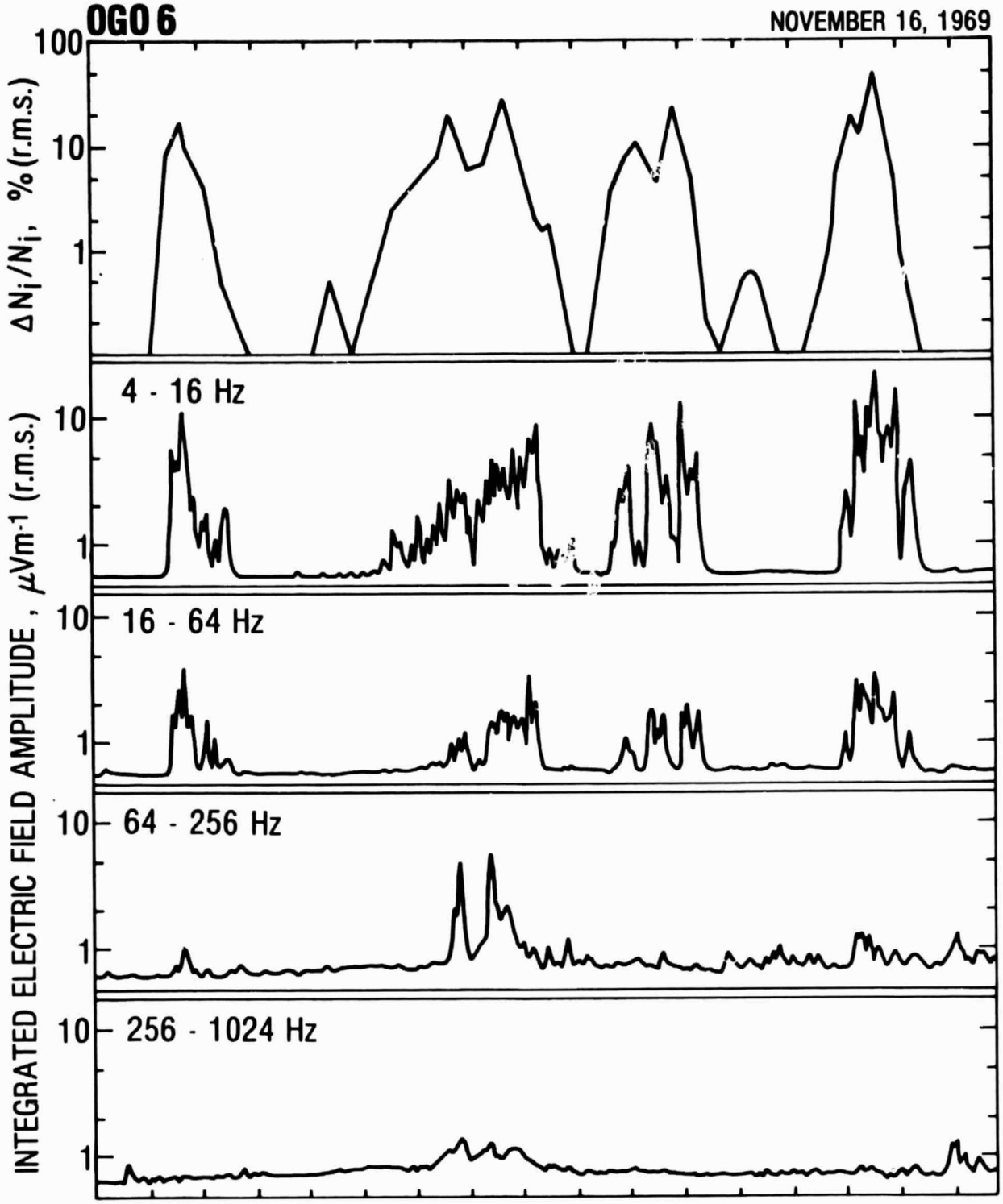
OGO 6
NOVEMBER 16, 1969
100
10
1
ΔNi/Ni, % (r.m.s.)
4 - 16 Hz
16 - 64 Hz
64 - 256 Hz
256 - 1024 Hz
INTEGRATED ELECTRIC FIELD AMPLITUDE, μVm-1 (r.m.s.)
UT 2115 2116 2117 2118 2119 2120 2121 2122
ALT (km) 405 401 398 397 398 400 404 410
MAG. LAT. 2.0 5.8 9.6 13.4 17.2 21.0 24.8 28.5
L 1.096 1.070 1.055 1.053 1.063 1.087 1.128 1.189

Figure 12

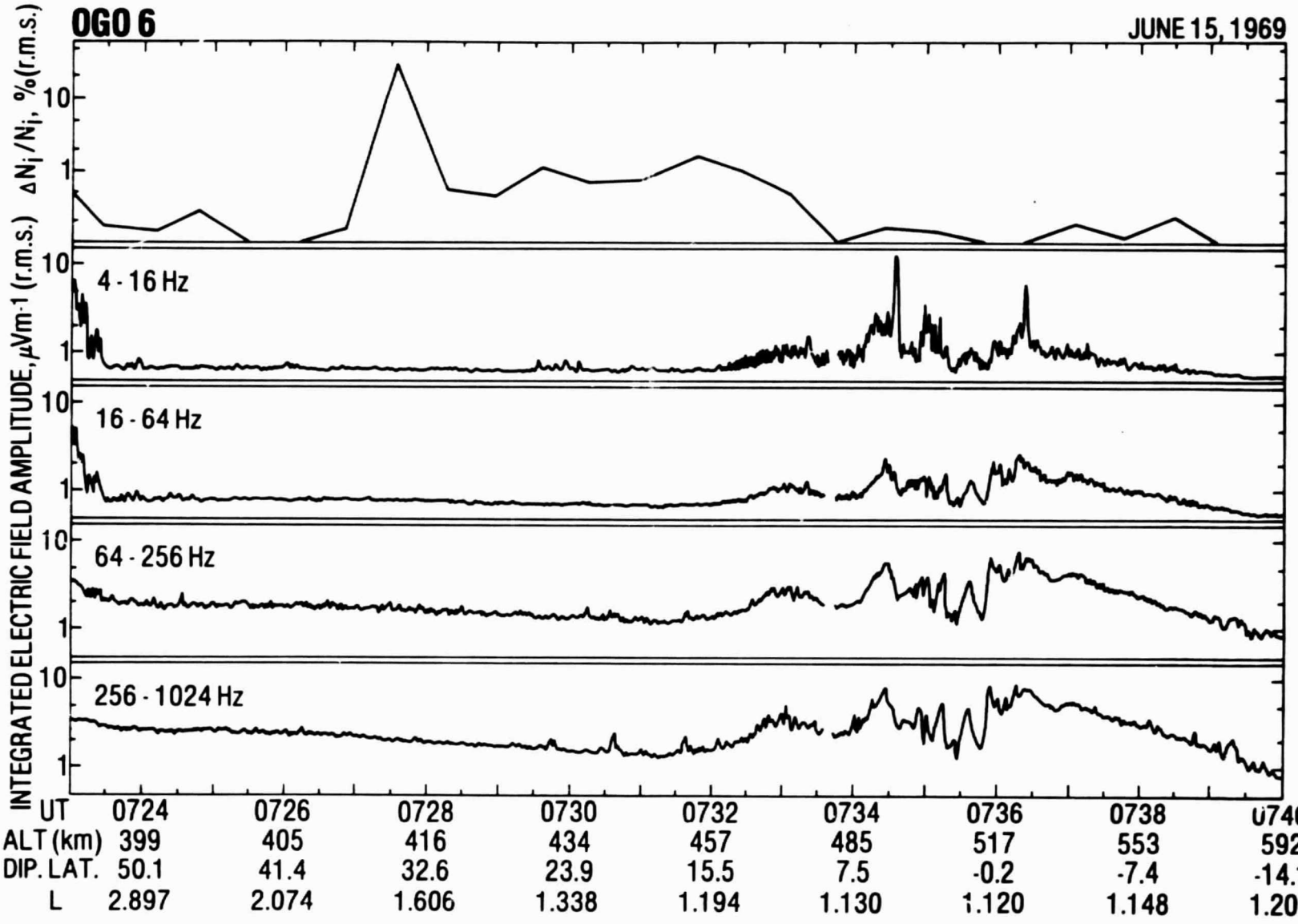
OGO 6
JUNE 15, 1969
INTEGRATED ELECTRIC FIELD AMPLITUDE, μVm⁻¹ (r.m.s.) ΔNi/Ni, %(r.m.s.)
10
1
4 - 16 Hz
16 - 64 Hz
64 - 256 Hz
256 - 1024 Hz
UT 0724 0726 0728 0730 0732 0734 0736 0738 0740
ALT (km) 399 405 416 434 457 485 517 553 592
DIP. LAT. 50.1 41.4 32.6 23.9 15.5 7.5 -0.2 -7.4 -14.1
L 2.897 2.074 1.606 1.338 1.194 1.130 1.120 1.148 1.207

Figure 13

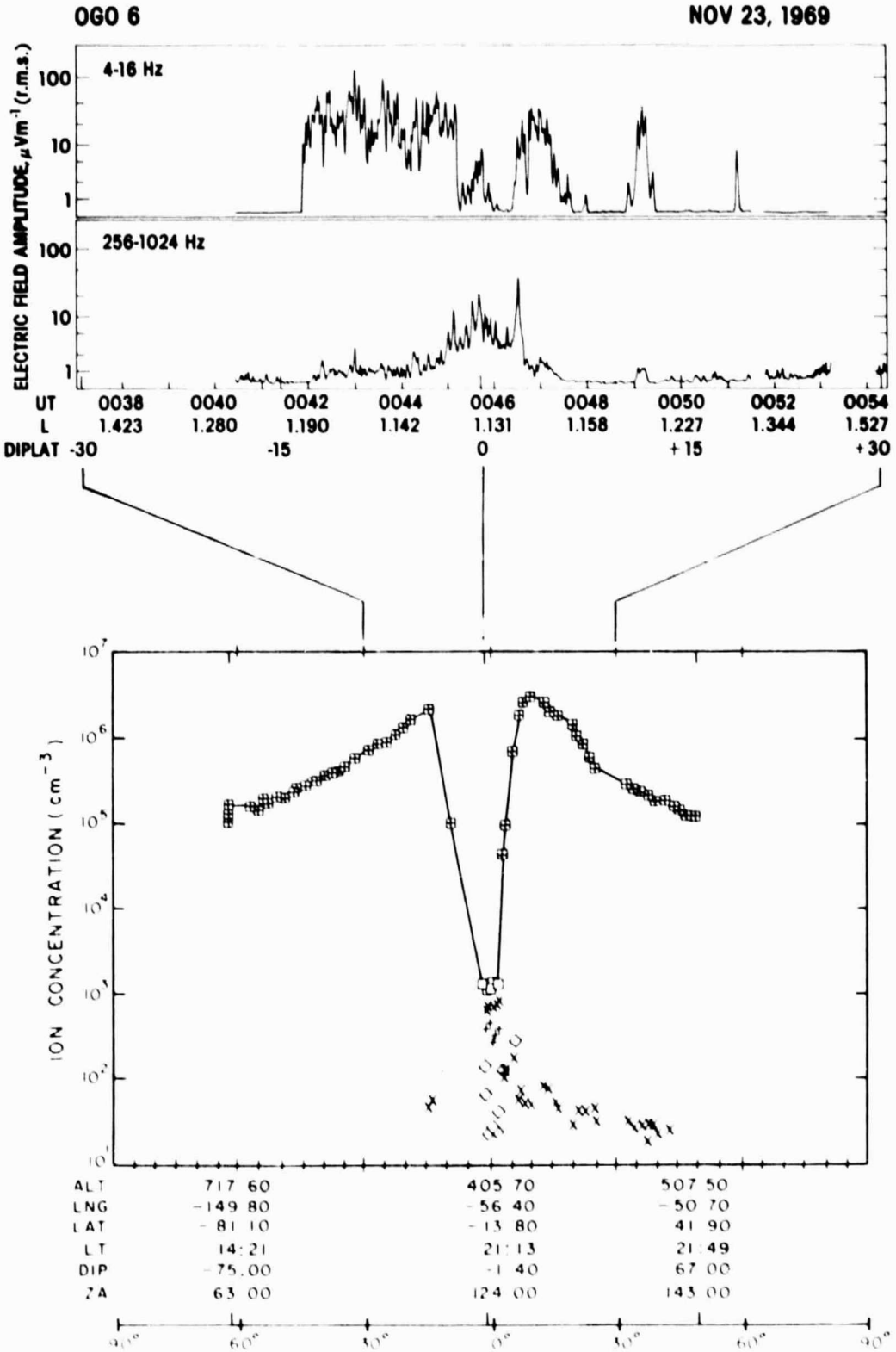
OGO 6
NOV 23, 1969
4-16 Hz
256-1024 Hz
ELECTRIC FIELD AMPLITUDE, μVm⁻¹ (r.m.s.)
100
10
1
UT 0038 0040 0042 0044 0046 0048 0050 0052 0054
L 1.423 1.280 1.190 1.142 1.131 1.158 1.227 1.344 1.527
DIPLAT -30 -15 0 +15 +30
ION CONCENTRATION (cm⁻³)
ALT 717 60 405 70 507 50
LNG -149 80 -56 40 -50 70
LAT -81 10 -13 80 41 90
LT 14:21 21:13 21:49
DIP -75.00 -1 40 67 00
ZA 63 00 124 00 143 00
90° 60° 30° 0° 30° 60° 90°

Figure 14